# Photoproduction of the $\phi$ meson off the deuteron near threshold

A. I. Titov[1,2] and B. Kämpfer[1,3]
[1]*Forschungzentrum Dresden-Rossendorf, D-01314 Dresden, Germany*
[2]*Bogoliubov Laboratory of Theoretical Physics, JINR, Dubna, RU-141980 Russia*
[3]*Institut für Theoretische Physik, TU Dresden, D-01062 Dresden, Germany*
(Received 14 May 2007; published 4 September 2007)

We discuss coherent and incoherent $\phi$ meson photoproduction off the deuteron at low energy and small momentum transfer with the aim of checking whether the recent experimental data need for their interpretation an inclusion of exotic channels. Our analysis of the differential cross section and spin-density matrix elements shows that new data on the $\gamma D \to \phi X$ reaction at $E_\gamma \sim 2$ GeV may be understood on the basis of conventional dynamics. However, a certain ambiguity of the deviation between the model predictions and the data from the laser electron photon beamline at SPring-8 (LEPS) on the $\gamma p \to \phi p$ reaction still remains. To make a firm conclusion about a possible manifestation of exotic channels, one has to improve the resolution of the data by providing additional information on the channels with spin- and double-spin-flip transitions which are sensitive to the properties of the photoproduction amplitude in the $\gamma p$ and $\gamma D$ reactions. This information may be used as an additional independent test of the $\phi$ meson photoproduction mechanism.

DOI: 10.1103/PhysRevC.76.035202 PACS number(s): 13.88.+e, 13.60.Le, 14.20.Gk, 25.20.Lj

## I. INTRODUCTION

The investigation of $\phi$ meson photoproduction at low energies, $E_\gamma \simeq 1.6$–3 GeV, plays an important role in understanding the nonperturbative Pomeron exchange dynamics and the nature of the $\phi N$ interaction. It was expected that in the diffractive region the dominant contribution comes from the Pomeron exchange, since the processes associated with conventional meson (quark) exchanges are suppressed by the Okubo-Zweig-Iizuka (OZI) rule [1–7]. An example of such a (suppressed) process is the pseudoscalar $\pi$ and $\eta$ meson exchange which, as a rule, was considered as a small correction to the dominant Pomeron exchange channel. The Pomeron exchange amplitude is usually described in terms of the Donnachie-Landshoff model [8], where the Pomeron couples to single constituent quarks as a $C = +1$ isoscalar photon, or a two gluon modification there of [6,9,10]. These models are designed for the vector meson photoproduction at high energy and small momentum transfer. The validity of an extrapolation of these models into the low energy region and close to the threshold is not clear. Near threshold, the models predict a monotonic increase of the differential cross section of the $\gamma p \to \phi p$ reaction at forward photoproduction angle with energy. However, a recent analysis of the $\phi$ photoproduction at low energy by the LEPS Collaboration shows a sizable deviation from this prediction; in particular, the data show a bump structure around $E_\gamma \simeq 2$ GeV [11]. Another peculiarity of the data from the laser electron photon beamline at SPring-8 (LEPS) is a strong deviation of the spin-density matrix element $\rho^1_{1-1}$ from 0.5, which is in favor of a sizable contribution of unnatural parity exchange processes. These facts raise several questions: (i) does one have to modify the conventional Pomeron exchange model at low energy, (ii) what is the source of unnatural parity exchange channels, and (iii) do we need to introduce some exotic channels (additional Reggeon trajectories, processes associated with possible hidden strangeness in the nucleon, etc.) to describe the data. In principle, these questions are related to each other and have to be analyzed simultaneously. Thus, for example, the mentioned bumplike behavior may be a result of the interplay of the pseudoscalar exchange amplitude and modified Pomeron exchange channels.

The coherent $\phi$ photoproduction off the deuteron in the diffraction region seems to be very useful for such an analysis. First of all, the isovector $\pi$ meson exchange amplitude is eliminated in the case of the isoscalar target. Therefore, the appearance of the bumplike structure in the energy dependence of the differential cross section of the reaction $\gamma D \to \phi D$ would favor a modification of the conventional Pomeron exchange amplitude. The next step is an analysis of spin observables, in particular, the properties of the decay $\phi \to K^+K^-$ with unpolarized and polarized photon beams. The incoherent $\phi$ photoproduction in the $\gamma D \to \phi pn$ reaction allows one to extract observables of the $\gamma n \to \phi n$ reaction which can be used for a simultaneous analysis of photoproduction off the neutron and proton targets in order to get additional and independent evidence of a manifestation of possible exotic channels.

Schematically, the coherent and incoherent $\phi$ meson photoproduction processes are exhibited in Fig. 1 with single and double scattering. The internal dashed lines in Figs. 1(b) and 1(d) correspond to diagonal ($m = \phi$) and nondiagonal ($m = \pi, \rho, \omega, \ldots$) transitions, respectively. In this paper, we study the $\phi$ meson photoproduction at low energies with $E_\gamma <$ 3 GeV at forward photoproduction angles with momentum transfer $|t| \lesssim 0.4$ GeV$^2$, where the single scattering processes are dominant. The coherent $\phi$ meson photoproduction at higher values of $|t|$ is controlled by the double scattering processes, which can provide important information about the cross section of the $\phi N$ scattering [12,13]. However, this interesting topic is beyond the scope of our present analysis, where we focus just on the extremely forward $\phi$ meson photoproduction, where some hint of an anomaly in the differential cross section of the $\gamma p \to \phi p$ reaction was found [11]. Some theoretical

 

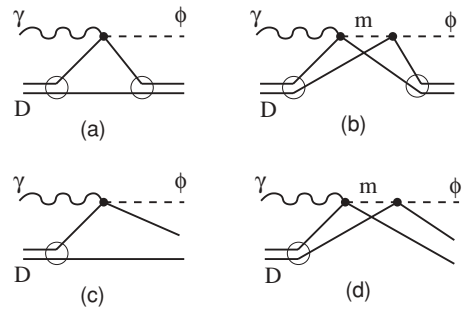


FIG. 1. Diagrammatic representation of coherent [(a), (b)] and incoherent [(c), (d)] $\phi$ meson photoproduction in the $\gamma D$ reactions with single [(a), (c)] and double [(b), (d)] scattering contributions.

estimate for the coherent vector meson photoproduction from the deuteron is given in Ref. [14]. The first experimental data on the $\gamma D \to \phi D$ reaction were reported recently in Refs. [15,16].

The aim of the present paper is to extend the results of Ref. [14] for the coherent and incoherent $\phi$ meson photoproduction off the deuteron and to give a consistent analysis of the recent experimental data on $\gamma D$ reactions to help determine whether they can be described in terms of conventional dynamics or whether some new (exotic) mechanisms are needed for their interpretation.

Our paper is organized as follows. In Sec. II we provide equations for the amplitudes of $\phi$ photoproduction off the proton which are used later for coherent and incoherent $\phi$ meson photoproduction in $\gamma D$ reactions. Here we also analyze the unpolarized differential cross section of the reaction $\gamma p \to \phi p$. In Sec. III we present a model for coherent and incoherent $\gamma D \to \phi X (X = D, np)$ reactions. In Sec. IV we provide a simultaneous analysis of spin-density matrix elements for $\phi \to K^+K^-$ decay distributions in $\gamma p, \gamma n$, and $\gamma D$ reactions. The summary is given in Sec. V.

## II. Φ MESON PHOTOPRODUCTION OFF THE PROTON

For the reaction $\gamma p \to \phi p$, we define the kinematic variables with the usual notation. The four-momenta of the incoming photon, outgoing vector meson, and initial and final protons are denoted as $k_\gamma, q_\phi, p$, and $p'$, respectively. The standard Mandelstam variables are defined as $t = (p' - p)^2 = (k_\gamma - q_\phi)^2, s \equiv W^2 = (p + k_\gamma)^2$.

In forward-angle photoproduction, the $s$ and $u$ channels with an intermediate nucleon and nucleon resonances are negligibly weak, and the main contribution comes from the Pomeron and pseudoscalar $(\pi, \eta)$ meson exchange processes. The corresponding model for the $\phi$ meson photoproduction in the $\gamma p \to \phi p$ reaction is described in Ref. [7]. However, for the sake of completeness in this section, we provide the main expressions for the invariant amplitudes which will be used below.

The photoproduction amplitude is expressed in standard form as

$$T^{\gamma p \to \phi p}_{m_f \lambda_\phi; m_i \lambda_\gamma} = \bar{u}_f \mathcal{M}_{\mu\nu} u_i \varepsilon^{*\mu}_{\lambda_\phi} \varepsilon^{\nu}_{\lambda_\gamma}, \tag{1}$$

where $\varepsilon_{\lambda_\gamma}$ and $\varepsilon_{\lambda_\phi}$ are the polarization vectors of the photon and $\phi$ meson, respectively, and $u_i = u_{m_i}(p)$ $[u_f = u_{m_f}(p')]$ is the Dirac spinor of the nucleon with momentum $p$ $[p']$ and spin projection $m_i$ $[m_f]$.

For the Pomeron exchange amplitude, we utilize the modified Donnachie-Landshoff (DL) model [8] to write

$$\mathcal{M}^{\mu\nu} = M(s,t)\Gamma^{\mu\nu}, \tag{2}$$

where the transition operator $\Gamma^{\mu\nu}$ reads

$$\Gamma^{\mu\nu} = \not{k}_\gamma \left( g^{\mu\nu} - \frac{q_\phi^\mu q_\phi^\nu}{q_\phi^2} \right) - \gamma^\nu \left( k_\gamma^\mu - q_\phi^\mu \frac{k_\gamma \cdot q_\phi}{q_\phi^2} \right) - \left( q_\phi^\nu - \frac{\bar{p}^\nu k_\gamma \cdot q_\phi}{\bar{p} \cdot k_\gamma} \right) \left( \gamma^\mu - \frac{\not{q}_\phi q_\phi^\mu}{q_\phi^2} \right), \tag{3}$$

with $\bar{p} = (p + p')/2$. The last term with $\bar{p}$ is added to restore the gauge invariance [7]. The scalar function $M_P(s,t)$ is described by the Reggeon parametrization

$$M_P(s,t) = C_P F_1(t) F_2(t) \frac{1}{s} \left( \frac{s}{s_P} \right)^{\alpha_P(t)} \exp\left[ -\frac{i\pi}{2} \alpha_P(t) \right], \tag{4}$$

where $F_1(t)$ is the isoscalar form factor of the nucleon and $F_2(t)$ is the form factor for the $\phi$ meson-photon-Pomeron coupling [8], that is,

$$F_1(t) = \frac{4M_N^2 - a_N^2 t}{(4M_N^2 - t)(1 - t/t_0)^2}, \qquad F_2(t) = \frac{2\mu_0^2}{(1 - t/M_\phi^2)(2\mu_0^2 + M_\phi^2 - t)}. \tag{5}$$

The Pomeron trajectory is known to be $\alpha_P(t) = 1.08 + 0.25t$. The strength factor $C_P$ is given by

$$C_P = \frac{6eg^2}{\gamma_\phi}, \tag{6}$$

where $\gamma_\phi \simeq 6.7$ is the $\phi$ meson decay constant. The parameter $g^2$ is a product of two dimensionless coupling constants $g^2 = g_{Pss} g_{Pqq} = (\sqrt{s_P}\beta_s)(\sqrt{s_P}\beta_u)$, where $g_{Pss}$ and $g_{Pqq}$ are Pomeron couplings with the strange quark in a $\phi$ meson and the light quark in a proton, respectively. In our study, we chose $t_0 = 0.7$ GeV$^2$, $\mu_0^2 = 1.1$ GeV$^2$, $s_P = 4$ GeV$^2$, and $\beta_s = 1.44$ and $\beta_{u(d)} = 2.04$ GeV$^{-1}$. The parameter $a_N = 2$ is taken to be larger than the corresponding parameter in the DL model [8], making the overall form factor close to that of the two-gluon exchange model [10]. Actually, the original DL model was motivated by the two-gluon exchange model of Landshoff and Nachtmann [17], therefore such a modification seems to be reasonable.

In the case of the pseudoscalar mesons exchange ($M = \pi, \eta$), the transition operator $\mathcal{M}_{\mu\nu}$ reads

$$\mathcal{M}^M_{\mu\nu} = -i \frac{e g_{\gamma\phi M} g_{MNN}}{M_\phi} \gamma_5 \frac{\varepsilon^{\mu\nu\alpha\beta} k_{\gamma\alpha} q_{\phi\beta}}{t - M_\pi^2} F_M^2(t), \tag{7}$$

with $g_{\pi NN} \simeq 13.26$, $g_{\gamma\phi\pi} \simeq -0.14$, and $g_{\gamma\phi\eta} \simeq -0.71$ [7]. In this paper, following estimates based on the QCD sum rule [18] and chiral perturbation theory [19], as well as the phenomenological analysis of $\eta$ photoproduction [20], we use

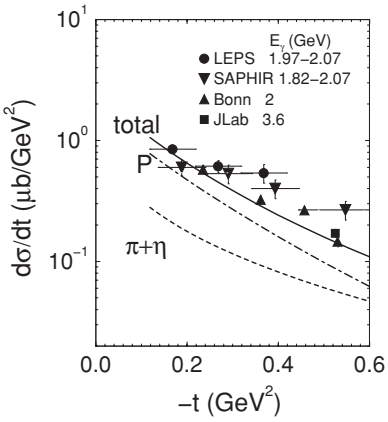


FIG. 2. Differential cross section of the $\gamma p \to \phi p$ reaction as a function of momentum transfer $t$ at $E_\gamma = 2.02$ GeV. The Pomeron and pseudoscalar exchange contributions and total cross section are shown by dot-dashed, dashed, and solid curves, respectively. Data are from LEPS [11], SAPHIR [22], Bonn [23], and JLab [24].

$g_{\eta NN} \simeq 1.94$. $F_M^2$ is the product of the two form factors of the virtual exchanged mesons in the $MNN$ and $\gamma VM$ vertices

$$F_M(t) = \frac{\Lambda_M^2 - m_\pi^2}{\Lambda_M^2 2 - t}, \tag{8}$$

with $\Lambda_{\pi(\eta)} = 1.05$ GeV. This value is slightly greater than the values of the cutoff parameters in Ref. [7] $\Lambda_{\pi(\eta)} = 0.6(0.9)$ GeV], which result in some modification of the pseudoscalar exchange contribution. The SU(3) symmetry predicts a constructive $\pi - \eta$ interference in $\gamma p$ reactions and a destructive interference in $\gamma n$ reactions [21].

In Fig. 2 we show the differential cross section of the $\gamma p \to \phi p$ reaction (solid curve) for the photon energy bin $E_\gamma = 1.97$–2.07 GeV from LEPS [11], together with the experimental data at $E_\gamma \sim 2$ GeV [11,22,23]. For completeness, we also display JLab [24] data, obtained at 3.6 GeV, because there is not much difference in the $t$ dependence of the Bonn [23] and JLab [24] data. One can see that the model satisfactorily describes the Bonn and JLab experimental data. However, it underestimates the LEPS and SAPHIR data at relatively large $|t|$ which probably may manifest additional channels beyond our simple model [7]. The energy dependence of the differential cross section at the forward photoproduction angle with $\theta = 0$ (i.e., $t = t_{\max}$) together with the experimental data [11] is shown in Fig. 3. One can see a sizable deviation of experimental data around $E_\gamma = 2.2$–2.4 GeV from the monotonic theoretical curve. Actually, it is a question of two data points for $E_\gamma = 2.17$–2.27 and 2.27–2.37 GeV energy bins [11] which are below the prediction based on the conventional dynamics. This deviation may indicate a manifestation of an additional exotic channel. On the other hand, it may be related to the difference between the $t$ dependences of different data sets. Thus, in Fig. 2 one can see a slightly different $t$ dependence of four different groups, which would result in a difference in $d\sigma(t = t_{\max})/dt$ found by an extrapolation to $t \to t_{\max}$.

It seems to be obvious that to understand the nature of this difference, one needs more precise experimental data at small energy bins not only on differential cross section but also on

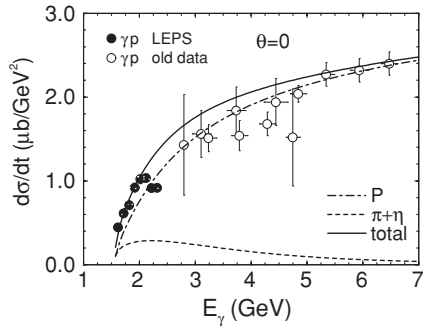


FIG. 3. Differential cross section of the $\gamma p \to \phi p$ reaction at $t = t_{\max}$ ($\theta = 0$) as a function of the photon energy. Experimental data are from Refs. [11,25].

polarization observables sensitive to the spin-flip channels. An additional way is to test an independent process at $E_\gamma \sim 2$ GeV for a manifestation of possible exotics. One of them is the coherent $\gamma D \to \phi D$ photoproduction [15] performed within the same experimental conditions as the $\gamma p \to \phi p$ reaction [11], which we consider below.

## III. Φ MESON PHOTOPRODUCTION IN $\gamma D$ REACTIONS

In this section, we consider coherent $\gamma D \to \phi D$ and incoherent $\gamma D \to \phi np$ photoproduction processes. The kinematic variables for these reactions are the following ones. The four-momenta of the initial and the final deuteron ($np$ system) are denoted as $p_D$ and $p'_X$ ($X = D, np$), respectively. The Mandelstam variables are defined as $s_D \equiv W_D^2 = (p_D + k_\gamma)^2$, $t_X = (p'_X - p_D)^2$, and so on. The space component of the momentum transfer to deuteron in the laboratory system is $\mathbf{q}^2 \equiv q^2 = -t_D(1 - t_D/4M_D^2)$, where $M_D$ is the deuteron mass.

### A. Coherent photoproduction

As mentioned above, here we consider the $\phi$ meson photoproduction at forward angles with $|t| \lesssim 0.4$ GeV$^2$, where the dominant contribution comes from the single scattering process, shown in Fig. 1(a). In such a case, one can use a nonrelativistic framework for the deuteron form factor based on utilizing the realistic $NN$ interaction. In our analysis, we use the deuteron wave function calculated with the Paris potential [26,27] designed just for describing nuclear processes at high momentum transfer. Thus, it describes fairly well the deuteron electromagnetic form factor with momentum transfer up to $-t \simeq 0.9$ GeV$^2$ [27].

The total vector meson photoproduction amplitude in the reaction $\gamma D \to VD$ reads

$$T^D_{M_f M_i;\lambda_V \lambda_\gamma} = 2 \sum_{\alpha\beta} \langle M_f \lambda_V, \beta | T^s_{\beta\alpha;\lambda_V \lambda_\gamma} | M_i \lambda_\gamma, \alpha \rangle, \tag{9}$$

where $M_i$, $M_f$, $\lambda_\gamma$, and $\lambda_V$ stand for the deuteron-spin projections of the initial and final states, and helicities of the incoming photon and the outgoing vector meson, respectively. $T^s$ is the amplitude of the vector meson photoproduction from

the isoscalar nucleon, i.e.,

$$T^s \equiv \tfrac{1}{2}(T^p + T^n). \tag{10}$$

The indices $\alpha$ and $\beta$ in Eq. (9) refer to all quantum numbers before and after the collision. The elementary photoproduction amplitudes $T^{p,n}$ were defined in the previous section. $\pi$ exchange terms are canceled in the total amplitude, since $T^n_\pi = -T^p_\pi$.

Using the standard decomposition of the deuteron state in terms of $s$ ($U_0$) and $d$ ($U_2$) wave functions, one can rewrite Eq. (9) in the explicit form

$$\begin{aligned} T^D_{M_f,M_i;\lambda_V\lambda_\gamma}(t) = 2\sqrt{4\pi}\sum i^\lambda \frac{\widehat{L'}\widehat{\lambda}}{\widehat{L}} Y_{\lambda\mu}(\widehat{\mathbf{q}}) C^{1M}_{\frac{1}{2}m_1\frac{1}{2}m} \\ \times C^{1M'}_{\frac{1}{2}m'_1\frac{1}{2}m} C^{1M_i}_{1MLM_L} C^{1M_f}_{1M'L'M_{L'}} \\ \times C^{LM_L}_{L'M_{L'}\lambda\mu} C^{L0}_{L'0\lambda0} R_{LL'\lambda}(q^2) T^s_{m_1m'_1;\lambda_V\lambda_\gamma}(t), \end{aligned} \tag{11}$$

where $\widehat{j} = \sqrt{2j+1}$, and the radial integral $R_{LL'\lambda}$ reads

$$R_{LL'\lambda}(q^2) = \int dr U_L(r) U_{L'}(r) j_\lambda(qr/2). \tag{12}$$

For a qualitative analysis of the unpolarized differential cross section at small momentum transfer with $\theta_{\hat{\mathbf{q}}} \simeq 0$, keeping only the spin/helicity conserving terms with natural $T^{\mathrm{N}}$ and unnatural $T^{\mathrm{U}}$ parity exchange in the total amplitude, one gets

$$T^{\mathrm{N}}_{mm';\lambda_V\lambda_\gamma}(t) = \begin{pmatrix} 1 \\ 2m\lambda_\gamma \end{pmatrix} \delta_{mm'}\delta_{\lambda_\gamma\lambda_V} T^{\mathrm{N}}_0(t). \tag{13}$$

Here, $T^{\mathrm{N}}_0(t)$ is the spin-independent part of the amplitudes. Using Eq. (11) with Eq. (13), we get the following result for the natural and unnatural parity-exchange parts of the total amplitude:

$$\begin{aligned} T^{D\mathrm{N}}_{M_fM_i;\lambda_V\lambda_\gamma} &= 2\delta_{M_iM_f}\delta_{\lambda_\gamma\lambda_V}(\delta_{\pm1M_i} S^{\mathrm{N}}_1 + \delta_{0M_i} S^{\mathrm{N}}_0) T^{\mathrm{N}}_0, \\ T^{D\mathrm{U}}_{M_fM_i;\lambda_V\lambda_\gamma} &= 2M_i\lambda_\gamma\delta_{M_iM_f}\delta_{\lambda_\gamma\lambda_V}\delta_{\pm1M_i} S^{\mathrm{U}}_1 T^{\mathrm{U}}_0. \end{aligned} \tag{14}$$

The form factors $S^{N,U}_i$ read

$$\begin{aligned} S^N_1 &= F_C - \sqrt{2}F_Q, \\ S^N_0 &= F_C + 2\sqrt{2}F_Q, \\ S^U_1 &= F_M, \end{aligned} \tag{15}$$

with

$$\begin{aligned} F_C &= R_{000} + R_{220}, \quad F_Q = R_{202} - \frac{1}{\sqrt{8}}R_{220}, \\ F_M &= R_{000} - \frac{1}{2}R_{220} + \sqrt{2}R_{202} + R_{220}. \end{aligned} \tag{16}$$

Taking into account the cancellation of the unnatural parity $\pi$ exchange contribution and neglecting weak $\eta$ meson exchange, one can express the differential cross section of the $\gamma D \to \phi D$ reaction by the cross section of the $\phi$ photoproduction from the isoscalar nucleon $\langle N\rangle$ as

$$\frac{d\sigma^{\gamma D}}{dt} \simeq 4Z(t)\frac{d\sigma^{\gamma\langle N\rangle}}{dt}, \tag{17}$$

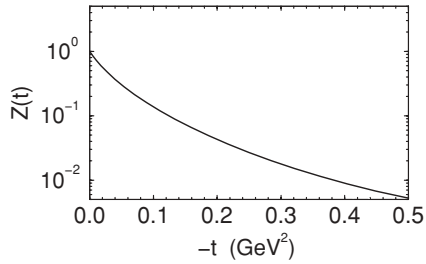


FIG. 4. Dependence of the structure factor $Z$ on $t = t_D$.

where $t = t_D$, and $Z(t)$ is the structure factor

$$Z(t) = F^2_C(t) + 4F^2_Q(t). \tag{18}$$

The dependence of $Z$ and $F_{C,Q}$ on $t_D$ is rather symbolic. In fact, these factors depend on the spatial part of the four-momentum transfer in the laboratory system $q$, as follows from Eq. (12). The relation between $t_D$ and $q^2$ reads $t_D = -2M_D(\sqrt{q^2 + M^2_D} - M_D)$. The structure factor $Z$ as a function on $t_D$ is shown in Fig. 4. In the considered region of momentum transfer $t$, the factor $Z(t)$ is related to the well-known structure function $A(t)$ of the elastic $eD \to eD$ scattering as

$$A(t) \simeq Z(t)G^2_d(t), \tag{19}$$

where $G_d(t) = 1/(1 - t/0.71)^2$ is the dipole electromagnetic form factor of the proton.

Equation (17) allows one to extract the cross section of the $\gamma\langle N\rangle$ reaction from the measured cross section of the $\gamma D$ reaction as

$$\frac{d\sigma^{\gamma\langle N\rangle}}{dt} \simeq [4Z(t)]^{-1}\frac{d\sigma^{\gamma D}}{dt}. \tag{20}$$

In Fig. 5 the differential cross section of the $\gamma D \to \phi D$ reaction is exhibited as calculated by using the explicit expression for the photoproduction amplitude given by Eq. (9), together with the available experimental data by LEPS [15] and CLAS [16] collaborations. For simplicity, we show only a comparison for the bin $E_\gamma = 2.07$–$2.17$ GeV. The description of the data for other bins has a similar quality. One can see that the model describes rather well the data at low momentum transfers $|t_D|$ but tends to underestimate the data

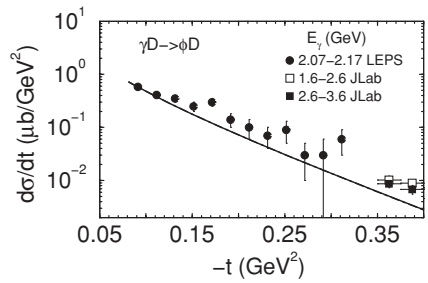


FIG. 5. Differential cross section of the $\gamma D \to \phi D$ reaction as a function of momentum transfer $t$ ($t = t_D$), with LEPS [15] and CLAS [16] data.

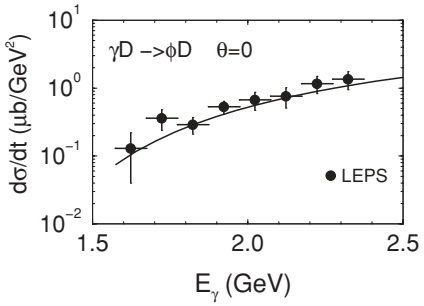


FIG. 6. Differential cross section of the $\gamma D \to \phi D$ reaction at $t = t_{\max}$ ($t = t_D$) as a function of the photon energy. Experimental data are from Ref. [15].

at higher $|t|$, probably pointing to the growing weight of more complicated (such as double scattering) channels.

In Fig. 6 we show the energy dependence of the differential cross section of the $\gamma D \to \phi D$ reaction at $\theta = 0$ (i.e., $t = t_{\max}$) together with experimental data [15]. The agreement between data and model is fairly reasonable. Note that here the experimental data do not point to a bumplike structure at $E_\gamma \sim 2$ GeV.

In Fig. 7 the comparison of $\phi$ meson photoproduction off the proton and off the isoscalar nucleon in a deuteron at $\theta = 0$ is displayed. In the latter case, the experimental data and the theoretical curve are evaluated from the corresponding cross section of the $\gamma D \to \phi D$ reaction by using Eq. (20). The figure displays the energy dependence of the differential cross sections at $\theta = 0$. One can see that the two cross sections are close to each other at all energies. The Pomeron exchange amplitude dominates at high energies. At lower energy, the behavior of the cross sections of the $\gamma p$ and $\gamma \langle N \rangle$ reactions is not trivial. The elimination of the isovector $\pi$ exchange contribution in the $\gamma \langle N \rangle$ reaction is compensated by a modification of momentum transfer $t$, which is smaller than that of the $\gamma p$ reaction near the threshold in the $\gamma D$ reaction. This causes the approach of both curves with decreasing energy $E_\gamma$.

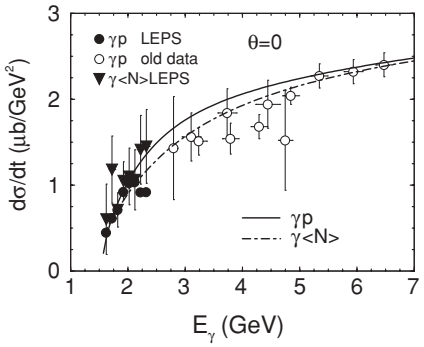


FIG. 7. Differential cross section of $\phi$ meson photoproduction off the proton (solid curve) and off the isoscalar nucleon in the $\gamma D$ reaction. Experimental data are from Refs. [11,15].

### B. Incoherent photoproduction

The main purpose of the measurement and the theoretical study of the incoherent $\phi$ meson photoproduction in the $\gamma D$ reactions is to extract the cross section of $\gamma n \to \phi n$ photoproduction with the goal of a subsequent combined analysis of $\gamma p$ and $\gamma n$ reactions to seek for a possible manifestation of exotic channels. This problem seems not too difficult if one uses the exclusive $\gamma D \to \phi np$ reaction. But at low energy and forward photoproduction angles, the momenta of the recoil nucleons are small, and there is an experimental problem with their detection. Therefore, another way is to study the $[\gamma D, \phi]$ missing mass distribution in the inclusive $\gamma D \to \phi X$ ($X = np, D$) reaction. Below we develop a model which can be used for the extraction of the observables of $\gamma n \to \phi n$ photoproduction.

The differential cross section of the $\phi$ meson photoproduction in the $\gamma D \to \phi np$ reaction reads

$$\frac{d\sigma}{dt dM_X} = \frac{1}{64\pi E_\gamma^2 M_D^2} \int d\widetilde{\Omega} \frac{\widetilde{p}}{16\pi^3} (|T_p|^2 + |T_n|^2), \quad (21)$$

where $\widetilde{p}$ and $\widetilde{\Omega}$ are the momentum and the solid angle of the spectator nucleon in the rest frame of the $np$ pair, respectively; $M_X$ is the invariant mass of this pair, and $t = t_X$; averaging and summing over the spin projections in the initial and the final states are assumed. $T_{p(n)}$ is the amplitude of the partial proton (neutron) contribution. It is related to the amplitude of the $\gamma N \to \phi N$ ($N = n, p$) reaction and the deuteron wave function $\psi^D$ as

$$T_N = -\sqrt{2M_D} \sum_{L\Lambda} \left\langle \frac{1}{2} m_2 \frac{1}{2} \bar{m} | 1 M_i - \Lambda \right\rangle \times \langle L\Lambda 1 M_i - \Lambda | 1 M_i \rangle T^{\gamma N \to \phi N}_{m_1 \lambda_\phi; \bar{m} \lambda_\gamma} \psi^D_{L\Lambda}(\mathbf{p}_s), \quad (22)$$

with

$$\psi^D_{L\Lambda}(\mathbf{p}) = (2\pi)^{\frac{3}{2}} i^L Y_{L\Lambda}(\widehat{\mathbf{p}}) u_L(p), \qquad u_L(p) = \sqrt{\frac{2}{\pi}} \int dr r U_L(r) j_L(pr), \quad (23)$$

where $p_s$ is the spectator momentum in the laboratory system, $u_L(r)$ is the radial deuteron wave function in the configuration space, $M_i$, $\lambda_\gamma$, $m_{1,2}$, and $\lambda_\phi$ are the spin projections of the incoming deuteron, photon helicity, the spin projections of the outgoing nucleons, and the helicity of the $\phi$ meson, respectively. For evaluating Eq. (21), we define kinematic variables by the following steps. For given $M_X$, the energy of the outgoing nucleons in the $np$ rest frame is $\widetilde{E} = M_X/2$. Then, using $\widetilde{\Omega}$ and the $\phi$ meson photoproduction angle in the center-of-mass system as input variables, we evaluate the four-momenta of the outgoing nucleons first in c.m.s. and then in the laboratory system. The four-momentum of the struck nucleon is $p_i = p_D - p_s$, where $p_D = (M_D, \mathbf{0})$. The amplitude $T^{\gamma N}$ in Eq. (11) is evaluated with an off-shell struck nucleon with $0 < p_i^2 < M_N^2$. In such a way, the off-shell effects in the incoherent channel are evaluated consistently.

The differential cross sections of the incoherent $\phi$ meson photoproduction are displayed in Figs. 8 and 9. Let us first discuss the differential missing mass distribution in the

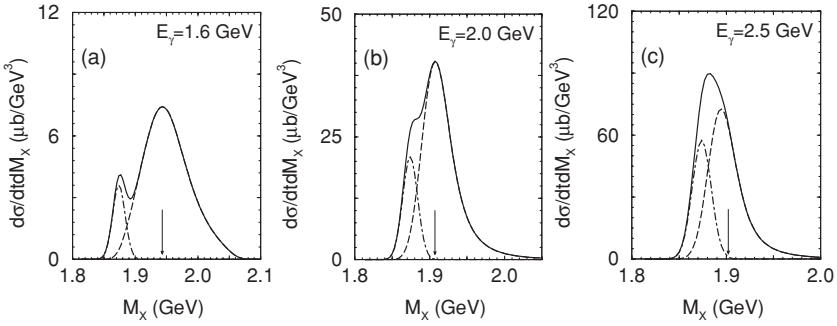


FIG. 8. Differential distribution of $[\gamma D, \phi]$ missing mass in $\gamma D \to \phi X$ reactions at different energies. The curves correspond to the cross sections of incoherent $\gamma D \to \phi(pn)$ (dashed) reactions, the coherent $\gamma D \to \gamma D$ (dot-dashed), and their sum (solid). The arrows mark the position of the maximum of the missing mass distribution.

$\gamma D \to \phi X$ reaction ($X = D, np$) as a function of the $[\gamma D, \phi]$ missing mass and momentum transfer $t$. For the coherent and incoherent parts, we use the common momentum transfer $t = t_D$. This means that the incoherent part must be multiplied by the Jacobian $dt_X/dt_D = \sqrt{\lambda(s, M_X^2, M_\phi^2)/\lambda(s, M_D^2, M_\phi^2)}$. With regards to a comparison of our prediction with the experimental data, the experimental resolution must be included. Also, the cross section of the incoherent photoproduction is slightly modified. Therefore, we compare data with the missing mass distribution folded with a Gaussian distribution function

$$\frac{d\sigma}{dM_X dt} = \int \frac{d\sigma}{dM dt} f(M_X - M) dM,$$
$$f(M_X - M) = \frac{1}{\sigma\sqrt{2\pi}} \exp\left[-\frac{(M_X - M)^2}{2\sigma^2}\right], \tag{24}$$

with $\sigma = 10$ MeV [15], which imitates a finite experimental resolution.

In Fig. 8, we show the differential $[\gamma D, \phi]$ missing mass distribution in $\gamma D \to \phi X$ reactions for different photon energies for the forward photoproduction angle $\theta = 0$. The position of the maximum of the incoherent part is marked by an arrow. One can see a strong energy dependence of (i) the absolute value of the cross section, (ii) the relative contributions of the coherent and incoherent processes, and (iii) the position of the maximum of the incoherent part. At relatively large photon energies ($E_\gamma \sim 2.5$ GeV), our model predicts a strong overlap of coherent and incoherent parts, and the coherent photoproduction amounts to more than 30% of the total cross section. Our model seems to be an effective tool for isolating the coherent and incoherent parts with subsequent extraction of the $\phi$ photoproduction off the neutron.

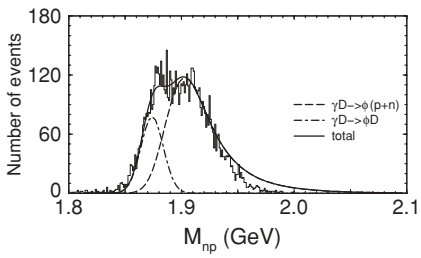


FIG. 9. Distribution of $[\gamma D, \phi]$ missing mass for the $\gamma D \to \phi X$ reaction. The histogram corresponds to the experimental data [28]. The theoretical curves are scaled by the factor 3.7 $(\mu\text{b/GeV}^3)^{-1}$ (see details in text).

Figure 9 exhibits the invariant mass distribution averaged within the interval $E_\gamma = 1.5$–$2.4$ GeV together with experimental data [28] given in units of events. The theoretical curves are scaled by the factor 3.7 $(\mu\text{b/GeV}^3)^{-1}$. The comparison is rather qualitative, because we did not use the detailed acceptance corrections which may somehow modify the shape of the distributions. Nevertheless, the qualitative agreement between prediction and data seems to be quite encouraging.

## IV. SPIN-DENSITY MATRIX ELEMENTS

In this section, we consider several important matrix elements of spin-density matrices $\rho^i_{\lambda\lambda'}$ ($i = 0, 1, 2$) which determine the $\phi$ meson decay distribution in its rest frame for both unpolarized and linearly polarized photon beams. The spin-density matrices are defined by

$$\rho^0_{\lambda\lambda'} = \frac{1}{N} \sum_{\alpha,\lambda_\gamma} T_{\alpha;\lambda,\lambda_\gamma} T^\dagger_{\alpha;\lambda',\lambda_\gamma},$$
$$\rho^1_{\lambda\lambda'} = \frac{1}{N} \sum_{\alpha,\lambda_\gamma} T_{\alpha;\lambda,-\lambda_\gamma} T^\dagger_{\alpha;\lambda',\lambda_\gamma}, \tag{25}$$
$$\rho^2_{\lambda\lambda'} = \frac{i}{N} \sum_{\alpha,\lambda_\gamma} T_{\alpha;\lambda,-\lambda_\gamma} T^\dagger_{\alpha;\lambda',\lambda_\gamma}.$$

The symbol $\alpha$ includes the polarizations of the incoming and outgoing baryons, and the normalization factor has the standard form

$$N = \sum_{\alpha,\lambda,\lambda_\gamma} T_{\alpha;\lambda,\lambda_\gamma} T^\dagger_{\alpha;\lambda,\lambda_\gamma}, \tag{26}$$

where $T_{\alpha;\lambda,\lambda_\gamma}$ is the total $\phi$ meson photoproduction amplitude.

We perform our consideration in the $\phi$ meson rest frame with the quantization axis along the beam momentum, i.e., the Gottfried-Jackson (GJ) system. Other possible choices are the helicity (H) system with the quantization axis opposite to the recoil nucleon (deuteron) momentum in the $\gamma p$ ($\gamma D$) reaction, and the Adair (A) system, where the quantization axis is along the beam direction in the c.m.s. [29]. The GJ system has some advantage because only here do some spin-density matrix elements have clear physical meanings, e.g., as a measure of the helicity conserving processes or as an asymmetry between processes with natural and unnatural parity exchange in the $t$ channel.

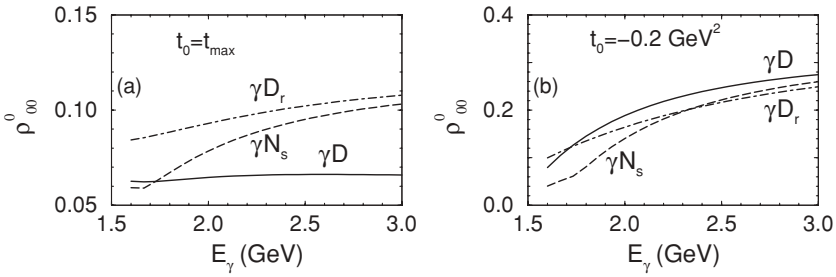


FIG. 10. Energy dependence of $\rho^0_{00}$ for the $\gamma D \to \phi D$ reaction at (a) $t_0 = t_{\max}$ and (b) $t_0 = -0.2$ GeV$^2$; $\Delta_t = 0.2$ GeV$^2$. Curves correspond to the explicit $\gamma D$ reactions (solid), the $\gamma D$ reaction with reduced cross sections (dot-dashed), and photoproduction off the free isoscalar nucleon (dashed).

Consider first the matrix element $\rho^0_{00}$. This matrix element determines the polar angular distribution of $\phi \to K\bar{K}$ decay

$$W(\cos\Theta) = \tfrac{3}{2}\left(\rho^0_{00} + \tfrac{1}{2}\left(1 - 3\rho^0_{00}\right)\sin^2\Theta\right). \tag{27}$$

In the GJ system, $\rho^0_{00}$ is the measure of the spin-flip transition with $\lambda_\gamma = \pm 1 \to \lambda_\phi = 0$. Thus, in the case of a pure helicity conserving amplitude, which may be expressed as

$$T_{\alpha;\lambda_\phi,\lambda_\gamma} \simeq \left(\boldsymbol{\varepsilon}_{\lambda_\gamma} \cdot \boldsymbol{\varepsilon}^*_{\lambda_\phi}\right) T^0_\alpha, \tag{28}$$

the photon polarization vector $\boldsymbol{\varepsilon}_{\lambda_\gamma}$ is transversal with respect to the $z$ axis, and therefore spin-flip transitions $\lambda_\gamma = \pm 1 \to \lambda_\phi = 0$ are forbidden, and $\rho^0_{00} = 0$, independently of the momentum transfer. In the helicity system, the photon polarization vector has a finite $z$ component

$$\varepsilon_{\lambda_\gamma z} = \frac{\lambda_\gamma}{\sqrt{2}}\sin\beta, \tag{29}$$

where $\beta$ is the angle between the H and GJ systems

$$\beta = \frac{v_\phi - \cos\theta}{v_\phi\cos\theta - 1}, \tag{30}$$

and $v_\phi$ and $\theta$ are the $\phi$ meson velocity and the $\phi$ photoproduction angle in c.m.s., respectively. For relatively large momentum transfer, when $\sin\beta \simeq 1$, one gets a large value of $\rho^{0\mathrm{H}}_{00}$

$$\rho^{0\mathrm{H}}_{00} \simeq \sin^2\beta, \tag{31}$$

even for the helicity conserving amplitude. Conversely, one can imagine an amplitude which generates $\rho^{0\mathrm{GJ}}_{00} \simeq 1$ [for example, take only the second term in Eq. (3)], and then $\rho^{0\mathrm{H}}_{00} \simeq \cos^\beta \simeq 0$. In general, the spin-density matrices in the H and GJ system are related to each other as

$$\rho^{i\mathrm{H}}_{\lambda\lambda'} = \sum_{\mu\nu} d^1_{\lambda\mu}(-\beta)\rho^{i\mathrm{GJ}}_{\mu\nu} d^1_{\nu\lambda'}(\beta). \tag{32}$$

Let us first discuss the energy dependence of the spin-density matrix element $\rho^0_{00}$ in the GJ system for $\gamma p$, $\gamma n$, and $\gamma D$ reactions. Following the experimental data, we calculate averaged $\rho$ matrices in the interval $|t| - |t_0| < \Delta_t$. The averaged $\rho$ matrices are defined as ratios of averaged numerators and denominators ($N$) in Eqs. (25). In such a case, a direct comparison of the $\rho$ matrices for the coherent $\gamma D$ and for the $\gamma p$ reactions is hampered by the deuteron form factor. The deuteron form factor drops rapidly with increasing values $-t$ (see Fig. 4) and, therefore, the dominant contributions in the $\gamma D$ and $\gamma p$ reaction at the same values of $t_0$ and $\Delta_t$ come from different momentum transfers $|\bar{t}_D| < |\bar{t}_p|$. This effect is particularly important for small values of $t_0 \simeq t_{\max}$, where the slope of the deuteron form factor is rather steep. Thus, at relatively large energies, say $E_\gamma \geqslant 2$ GeV, the main contribution comes from $|\bar{t}_D| \simeq |t_0| \sim 0$, making the averaged $\rho$ matrices for the $\gamma D$ reaction practically constant. One can remove the effect of the deuteron form factor by scaling the product $TT^\dagger$ in Eqs. (25) (or in the cross sections of the $\gamma D \to K^+K^-D$ reactions) by an inverse structure factor $Z(t)$ given by Eq. (18). Such reduced $\rho$ matrices would be much closer to the $\rho$ matrices for the photoproduction off the "free" isoscalar nucleon. Figure 10 illustrates the effect of the deuteron form factor for the $\gamma D$ reaction and the $\gamma D$ reaction with reduced cross sections. The latter one is denoted as $\gamma D_r$. For completeness, we also show results for the $\phi$ photoproduction off the free isoscalar nucleon. One can see a large difference between predictions for $\gamma D$ reaction and the photoproduction off the free isoscalar nucleon at $t_0 = t_{\max}$. In the first case, $\rho^0_{00}$ is almost constant, whereas in the second case it increases with energy in the given energy interval. Such an increase for the $\gamma N$ reaction can be understood as follows. The finite value of $\rho^0_{00}$ is generated by the Pomeron exchange amplitude and is determined by the second (main) and third terms in Eq. (3), whereas the total cross section is dominated by the first term. Neglecting spin-conserving pseudoscalar meson exchange, one can get the following analytical estimate of $\rho^0_{00}$ for the GJ frame for the pure Pomeron exchange channel:

$$\rho^0_{00\mathrm{approx}} \simeq \frac{2\left(2p_x^2 - t\right)k_\gamma^2}{\left(s - M_N^2\right)\left(s - M_N^2 - M_\phi^2 - t\right)}, \tag{33}$$

where $p_x$ is the $x$ component of the nucleon momentum ($p_x = p'_x$), $k_\gamma$ is the photon energy, and $s$ is the total energy squared in the $\gamma N$ vertex. At fixed $t$, dependence on form factors in numerator and denominator for the $\gamma N$ reaction is canceled. The increase of $\rho^0_{00}$ with energy, within the considered energy interval, is explained by a faster increase of the numerator (because of factor $p_x^2$) compared to the denominator at fixed $t$. At larger energies and small $|t|$, this ratio and the corresponding matrix element decrease.

The difference between the reduced $\rho^0_{00}$ matrix element and the case of photoproduction off the isoscalar nucleon is explained by the difference in $p_x, k_\gamma, t_{\max}$, and $s$ for $\gamma p$ and $\gamma D$ reactions. Actually, the kinematic variables in $\gamma N$ vertices in $\gamma p$ and $\gamma D$ reactions at fixed $E_\gamma$ and $t$ ($|t^d_{\max}| < |t^p_{\max}|$) are different, and this difference is reflected in spin-density matrix elements. As an illustration, in Fig. 11 we exhibit results for $\rho^0_{00}$ given as a ratio of the average numerator and denominator in Eq. (33) calculated for $\gamma p$ and $\gamma D$ kinematics. One can

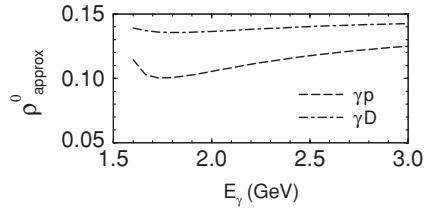


FIG. 11. Estimates of $\rho^0_{00}$ given by Eq. (33) for $\gamma p$ and $\gamma D$ reactions.

see some difference between the two cases caused by pure kinematics.

The comparison of $\rho^0_{00}$ for the $\gamma p$, $\gamma n$, and $\gamma D$ reactions without and with scaling by $Z^{-1}(t)$ is shown in Fig. 12. In Fig. 12(a) we show the result for forward photoproduction angles with $t_0 = t_{\max}$ ($\theta = 0$), together with available experimental data [11]. In Fig. 12(b) we choose the case of a larger momentum transfer with $t_0 = -0.2$ GeV$^2$ for each energy. One can see a monotonic increase of $\rho^0_{00}$ with energy, and the inequality $\rho^0_{00}(\gamma p) < \rho^0_{00}(\gamma n) < \rho^0_{00}(\gamma D_r)$ holds. Some enhancement of $\rho^0_{00}$ in $\gamma n$ reactions is explained by the destructive interference in the $\pi - \eta$ meson exchange amplitude which leads to a decrease of the helicity conserving terms in the full amplitude. Therefore, the relative contribution of the spin-flip terms in the $\gamma n$ reaction [cf. Eq. (3)] would be larger. In the $\gamma D_r$ reaction, together with a total suppression of $\pi$ meson exchange, $\rho^0_{00}$ increases additionally because of some difference in kinematics, as discussed above.

In Fig. 13 we exhibit the angular distribution $W(\cos\Theta)$ in the $\gamma D \to \phi D \to K^+K^-D$ reaction in the *helicity* frame for $E_\gamma = 3.1$ GeV and for $t_0 = -0.3$ GeV$^2$ together with available experimental data [16] given in this frame. The shown experimental data were obtained in two energy bins with $E_\gamma = 1.6$–$2.6$ and $2.6$–$3.6$ GeV and momentum transfer $|t| = 0.35$–$0.8$ GeV$^2$. In our calculation, the momentum transfer is in the range $|t| = 0.3$–$0.5$ GeV$^2$, which corresponds to an upper bound of the momentum transfer acceptable for our model for the $\gamma D \to \phi D$ reaction with single scattering processes. Nevertheless, one can see a reasonable agreement between calculation and data. Note that this distribution is different in different frames because of the frame dependence of the $\rho$ matrices. As an example, in Fig. 14 we show the energy dependence of $\rho^0_{00}$ for the $\gamma D \to \phi D$ reaction in the H and GJ frames at $|t| - |t_0| < 0.2$ GeV$^2$ and $-t_0 = 0.2$ GeV$^2$.

The energy dependence of the spin-density matrix element $\mathrm{Re}\rho^0_{1-1}$ is displayed in Fig. 15. This matrix element determines the azimuthal angle distribution of $\phi \to K\bar{K}$ decay in

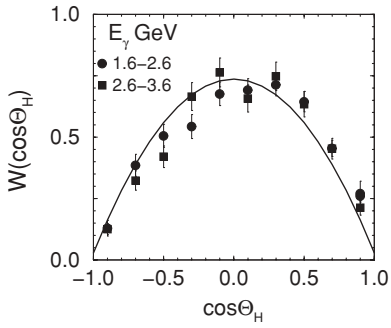


FIG. 13. Angular distribution $W(\cos\Theta)$ for the $\gamma D \to \phi D \to K^+K^-D$ reaction in the helicity frame at $E_\gamma = 3.1$ GeV and $-t_0 = 0.3$ GeV$^2$. Experimental data for two energy intervals and $|t| = 0.35$–$0.8$ GeV$^2$ are taken from Ref. [16].

reactions with an unpolarized photon beam

$$W^0(\Phi) = \frac{1}{2\pi}\left(1 - 2\mathrm{Re}\rho^0_{1-1}\cos 2\Phi\right). \tag{34}$$

In Fig. 15, we show results for $|t| - |t_0| < 0.2$ GeV$^2$ with $t_0 = t_{\max}$ and $t_0 = -0.2$ GeV$^2$ together with available experimental data [11]. The finite value of $\rho^0_{1-1}$ comes from the small component of the amplitude responsible for the double-spin transitions where the helicity of the $\phi$ meson differs from the helicity of the photon by two units: $\lambda_\gamma = \pm 1 \to \lambda_\phi = \mp 1$. In many models for $\phi$ photoproduction, such as scalar, pseudoscalar $t$-channel exchange, and the original DL Pomeron exchange model based on the Pomeron-isoscalar photon identity, these transitions are forbidden, and $\rho^0_{1-1}$ is exactly equal to zero. In the modified DL model, motivated by the two-gluon exchange dynamics, the term responsible for the double-spin transition [last term in Eq. (3)] arises naturally, because it also restores the gauge invariance of the original DL model. Therefore, the prediction of the finite value of $\rho^0_{1-1}$ is doubtless a success of this model. Interestingly, we get agreement in the $E_\gamma = 2.17$–$2.37$ GeV energy bin, while the model disagrees with the LEPS data on the unpolarized cross section. The model also differs from the data at $E_\gamma = 1.97$–$2.17$ GeV, whereas we just agree with the LEPS data on the unpolarized cross section in the $\gamma p$ reaction (cf. Fig. 3). This seems to be interesting. If one needs an exotics for the interpretation of the unpolarized data at $E_\gamma = 2.17$–$2.37$ GeV, then the question arises as to why it is not manifest in the delicate quantity $\rho^0_{1-1}$, and vice versa. Another problem is the following. The double-spin transition comes from the orbital interaction. Therefore, at fixed $t - t_{\max}$ it must be close to zero near the threshold and monotonically increase

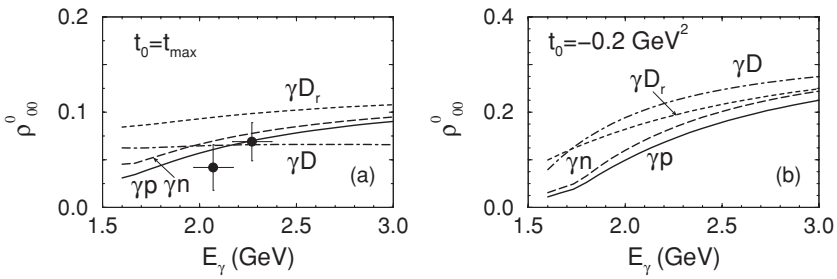


FIG. 12. Energy dependence of $\rho^0_{00}$ with (a) $t_0 = t_{\max}$ and (b) $t_0 = -0.2$ GeV$^2$ . Experimental data are from Ref. [11].

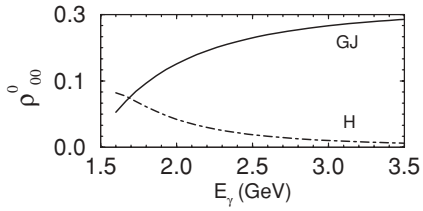


FIG. 14. Spin-density matrix elements $\rho^0_{00}$ in the helicity and Gottfried-Jackson frames at $|t| - |t_0| < 0.2$ GeV$^2$ and $t_0 = -0.2$ GeV$^2$.

with energy. This is a model-independent prediction, and it is in contradiction with the data, which show a decrease with energy. Such a strong violation of a general principle must be confirmed by independent measurements. Coming back to the result shown in Fig. 15, we note that the inequality $\rho^0_{1-1}(\gamma p) < \rho^0_{1-1}(\gamma n) < \rho^0_{1-1}(\gamma D)$ is similar to that in the previous case of single spin-flip transitions.

The matrix elements $\rho^{1,2}_{1-1}$ are related to the asymmetry of transitions with natural [first term of Eq. (3)] and unnatural $(\pi, \eta)$ parity exchange. They determine the $\phi$ meson decay distribution for linearly polarized photons as a function of the angle between the azimuthal decay angle $(\Phi)$ and the angle of the polarization plane $(\Psi)$

$$W^L(\Phi - \Psi) = \frac{1}{2\pi}\left[1 + 2P_\gamma \bar{\rho}^1_{1-1}\cos 2(\Phi - \Psi)\right], \quad (35)$$

where $P_\gamma$ is the strength of polarization, and

$$\bar{\rho}^1_{1-1} = \tfrac{1}{2}\left(\rho^1_{1-1} - \mathrm{Im}\rho^2_{1-1}\right) \simeq \rho^1_{1-1}. \quad (36)$$

The energy dependence of the spin-density matrix element $\bar{\rho}^1_{1-1}$ is shown in Fig. 16 together with the experimental data [11,15]. In this case, the effect of the deuteron form factor is rather weak, and we do not display results for the reduced matrix element. For pure natural (unnatural) parity exchange, it is equal to 0.5 $(-0.5)$. Qualitatively, within experimental accuracy, the result of our calculation is consistent with the data. Sizable deviations of $\bar{\rho}^1_{1-1}$ from 0.5 in the $\gamma p$ reaction at low energy are explained by a large contribution of the $\pi, \eta$ exchange processes. Thus, at $E_\gamma \simeq 2$ GeV they contribute on the level of 30% to the total cross section. In $\gamma n$ and $\gamma D$ reactions, the pseudoscalar exchange contributions are suppressed, shifting $\bar{\rho}^1_{1-1}$ toward 0.5.

For completeness, we also present the angular distribution $W^L(\Phi - \Psi)$ of Eq. (35) for different cases. Figure 17 exhibits this angular distribution for the reaction $\gamma p \to \phi p \to pK^+K^-$ at $|t| - |t_{\max}| \leqslant 0.2$ GeV$^2$ in the two energy intervals $E_\gamma = 1.97$–$2.17$ and $2.17$–$2.37$ GeV with beam polarization $P_\gamma = 0.86$ and $0.90$, respectively, together with available experimental data [30]. One can see a reasonable agreement between our calculation and the experiment.

The angular distribution $W^L(\Phi - \Psi)$ for the inclusive $\gamma D \to \phi X$ $(X = D, np)$ reaction is displayed in Fig. 18 together with the experimental data of Ref. [15]. This distribution is calculated using the model, developed in Sec. III. Figures 18(a) and 18(b) correspond to events with $[\gamma D, \phi]$ missing mass smaller or larger than $M_{\mathrm{cut}} = 1.89$ GeV, respectively. In the first case, the contributions come from both the coherent and incoherent $\phi$ meson photoproduction. The "effective" $\bar{\rho}^1_{1-1}$ matrix element is expressed as the sum

$$\bar{\rho}^{1L}_{1-1\mathrm{eff}} = \bar{\rho}^1_{1-1D}P_{CH} + \bar{\rho}^1_{1-1np}(1 - P_{CH}), \quad (37)$$

where $P_D$ is the relative weight of the coherent channel, and $\rho_{np} = (\rho_n + \rho_p)/2$ is the $\rho$ matrix for the quasifree nucleon. In the second case, the contribution of the coherent channel is negligible, and we get

$$\bar{\rho}^{1R}_{1-1\mathrm{eff}} \simeq \bar{\rho}^1_{1-1np}. \quad (38)$$

In Fig. 18, we show results for $|t| - |t_{\max}| < 0.1$ GeV$^2$ and the energy bin with $E_\gamma = 2.27$–$2.37$ GeV [15]. Here, the beam polarization is $P_\gamma = 0.935$ and the model predicts $P_{CH} \simeq 0.67$. One can see a sufficient agreement between the theoretical curves and the data. A similar agreement holds for the other energy bins.

The agreement between the experimental data and the calculations for the $K^+K^-$ angular distributions in $\gamma p$ and $\gamma np$ reactions means that the model describes correctly the $\phi$ photoproduction off the neutron, and in particular, supports our choice of the pseudoscalar channel with a small contribution of the $\eta$ meson exchange.

The sum $\rho^1_M \equiv 2\rho^1_{11} + \rho^1_{00}$ determines the $\phi$ meson decay distribution as a function of the angle between production and beam polarization planes, that is,

$$W^L(\Psi) = \frac{1}{2\pi}\left(1 + 2P_\gamma \rho^1_M \cos 2\Psi\right). \quad (39)$$

It is important that parity conservation requires $\rho^1_{\mu\nu} = (-1)^{\mu-\nu}\rho^1_{-\mu-\nu}$ [29], which makes $\rho^1_M$ invariant under rotation of the coordinate frame in the production plane. This means that $\rho^{1\mathrm{GJ}}_M = \rho^{1\mathrm{H}}_M = \rho^{1\mathrm{A}}_M$. Therefore, it is natural that this invariant function determines the distribution which depends only on the beam polarization.

Since $\rho^1_M$ is proportional to a combination of single and double-spin-flip transition amplitudes, its absolute value is small. The energy dependence of $\rho^1_M$ is shown in Fig. 19. One

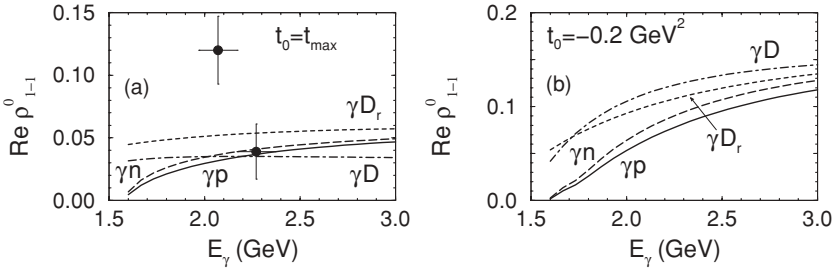


FIG. 15. Same as Fig. 12, but for Re$\rho^0_{1-1}$.

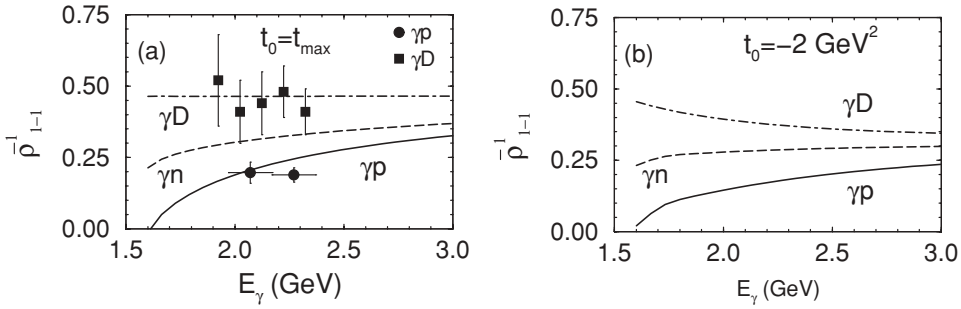


FIG. 16. Same as Fig. 12, but for $\rho^1_{1-1}$. Experimental data are from Refs. [11,15].

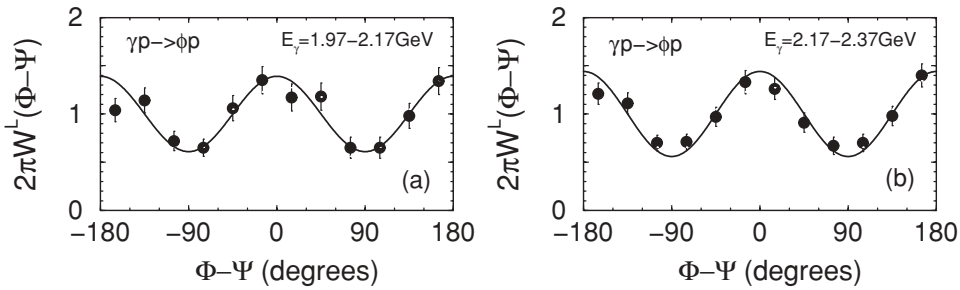


FIG. 17. Angular distribution $W^L(\Phi-\Psi)$ for the reaction $\gamma p \to \phi p \to p K^+ K^-$ at $|t| - |t_{max}| \leqslant 0.2$ GeV$^2$ for energy intervals (a) $E_\gamma = 1.97$–$2.17$ and (b) $E_\gamma = 2.17$–$2.37$ GeV. Experimental data are from Ref. [30].

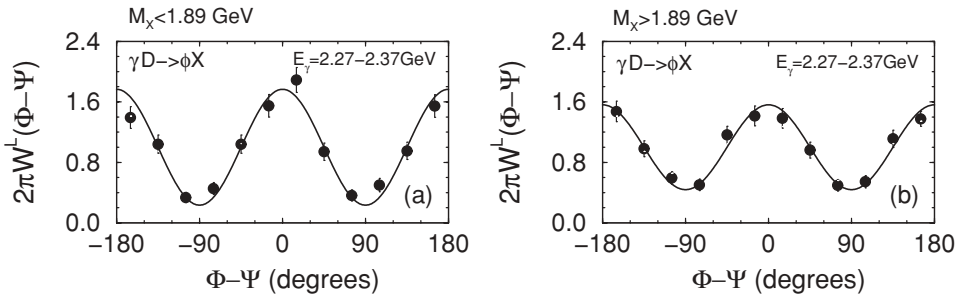


FIG. 18. Angular distribution $W^L(\Phi-\Psi)$ for the reaction $\gamma D \to \phi X \to X K^+ K^-$ ($X = D, np$) at $|t| - |t_{max}| \leqslant 0.1$ GeV$^2$. (a) and (b) correspond to the $[\gamma D, \phi]$ missing mass smaller or larger than 1.89 GeV, respectively. Experimental data are from Ref. [15].

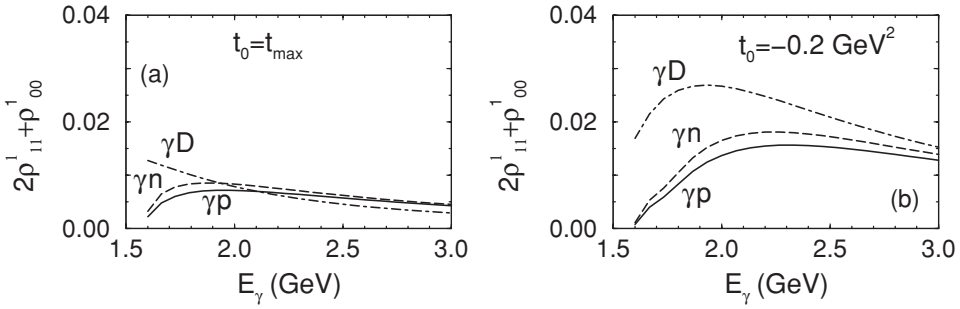


FIG. 19. Energy dependence of $2\rho^1_{11} + \rho^1_{00}$ for $t_0 = t_{max}$ and $t_0 = -0.2$ GeV$^2$.

can see some increase of $\rho^1_M$ when going from (a) $t_0 = t_{\max}$ to (b) $t_0 = -0.2$ GeV$^2$. This is explained by an increasing contribution of spin-flip transitions with $|t|$.

## V. SUMMARY AND DISCUSSION

We studied different aspects of coherent and incoherent $\phi$ meson photoproduction off the deuteron at forward photoproduction angles to check whether recent experimental data require the inclusion of some exotic channels discussed in literature. For this purpose, we reanalyzed the elementary $\gamma p \to \phi p$ reaction in order to use it as an input for our study. The corresponding amplitude in the diffractive region is expressed as a sum of Pomeron and pseudoscalar exchange channels. The first one represents a slightly modified Donnachie-Landshoff Pomeron exchange amplitude, whereas the second one is the coherent sum of the $\pi$ and $\eta$ meson exchange channels. In the present work, the contribution of the $\eta$ exchange channel is relatively weak, and correspondingly, the $\pi$ exchange is enhanced in order to get the proper relative contributions of the channels with natural and unnatural parity exchange. The Donnachie-Landshoff model is designed for high energy, and it is not clear whether it can also be applied at low energies or close to the threshold.

We performed a detailed analysis of the differential cross section of the $\gamma p \to \phi p$ reaction at $E_\gamma \sim 2$ GeV and obtained a reasonable agreement between the model predictions and the available experimental data in the diffraction region. At larger momentum transfer, our model underestimates the recent data of LEPS and SAPHIR but is quite reasonable for the Bonn and JLab data up to $t = 0.8$ GeV$^2$. However, this model cannot describe the deviation of two data points for $E_\gamma = 2.17$–$2.27$ and 2.27–2.37 GeV energy bins [11] from the monotonic curve predicted by the conventional dynamics. This is a subject for future studies. On the other hand, the Pomeron exchange model, motivated by the two-gluon dynamics, contains terms responsible for single and double-spin-flip transitions. The model predictions for the spin-density matrix elements being sensitive to the spin-flip transitions agree with the available data for the $\gamma p$ reaction at $E_\gamma \sim 2$ GeV, which also decreases the space left for possible exotic channels. Notice, however, that our model does not explain a large value of the $\rho^0_{1-1}$ spin-density matrix element at the $E_\gamma = 1.97$–$2.17$ GeV bin, being in agreement for the 2.17–2.37 GeV energy bin. The reported fast decreasing $\rho^0_{1-1}$ with energy contradicts the conventional knowledge that the orbital interaction responsible for the double-spin-flip transition must intensify with energy and lead to an increase of $\rho^0_{1-1}$. Therefore, we can conclude that for a clear understanding of a possible manifestation of an exotic channel, one needs a complete set of $t$ dependencies for the unpolarized cross sections and polarization observables at different energies as well.

We developed a model for the coherent and incoherent $\phi$ meson photoproduction off the deuteron and performed again a detailed analysis of the existing data. The slope of the differential cross section of the coherent $\phi$ meson photoproduction is defined by the corresponding slope of the elementary $\gamma N$ reaction and by the deuteron form factor. We found a quite reasonable agreement between the model prediction and the experimental data in the diffractive region and some underestimate at large $|t| \sim 0.4$ GeV$^2$, which favor the contributions of more complicated channels, for example, double scattering processes. But on the other hand, the model calculation of the $\phi \to K^+K^-$ decay distribution, $W(\cos\Theta)$, at $|t| \simeq 0.4$ GeV is in a good agreement with the experimental data, which, to some extent, support the single scattering model in this region of $t$. Therefore, the remaining difference between theory and experiment at $|t| \sim 0.4$ GeV$^2$ requires further investigation.

The model fairly well describes the energy dependence of the cross section of the $\gamma D \to \phi D$ reaction at $\theta = 0$ without any hint of a bumplike behavior.

We performed detailed and combined investigation of several important spin-density matrix elements for $\gamma p \to \phi p$, coherent $\gamma D \to \phi D$, and incoherent $\gamma D \to \phi np$ reactions aimed at (i) studying the effect of elimination of the isovector $\pi$ meson exchange in the coherent $\gamma D$ reaction and (ii) extracting observables for the $\gamma n$ reaction. The elimination of the $\pi$ meson exchange has two consequences. One is the relative decrease of channels with spin-conserving amplitudes, which results in an increase of the relative contributions of the spin-flip transitions. This leads to an enhancement of the corresponding spin-density matrix elements. Another consequence is related to a strong suppression of the amplitude with unnatural parity exchange and shift of the $\rho^1_{1-1}$ matrix element toward 0.5. We obtained a common description of $\phi$ meson decay distributions for $\gamma p \to \phi p$ and incoherent $\gamma D \to \phi np$ reactions, confirming the reliability of our model for the $\gamma n$ reaction.

To summarize, we can conclude that the existing experimental data (including also very recent data) on $\gamma p$, coherent $\gamma D \to \phi D$, and incoherent $\gamma D \to \phi np$ reactions in the diffraction region at low energies support the model based on the dominance of the Donnachie-Landshoff Pomeron plus $\pi$, $\eta$ exchange channels with a relatively weak $\eta$ meson contribution. An exception is the difference in the $\rho^0_{1-1}$ spin-density matrix element in the $E_\gamma = 1.97$–$2.17$ GeV bin discussed above and the deviation of two data points in the unpolarized cross section from the monotonic curve based on conventional dynamics in the $\gamma p \to \phi p$ reaction (bumplike behavior). But on the other hand, there in no such behavior in the familiar $\gamma D$ reaction, analyzed within the same experimental conditions. The question is why? If one could suggest that this bump is a result of the interference of large isoscalar and isovector ($\pi$ meson exchange) amplitudes with unnatural parity exchange in the $\gamma p$ reaction, then it would be in contradiction with the $\rho^1_{1-1}$ matrix element in the $\gamma D$ reaction which almost completely eliminates the admixture of the isoscalar unnatural parity exchange amplitude. A possible explanation of the exotics is the large admixture of an amplitude with properties of the isovector scalar $a_0$ meson exchange which can interfere with the Pomeron amplitude in the $\gamma p$ reaction and disappears in the coherent $\gamma D$ reaction. The effect of such interference should also be seen in the shape of unpolarized $\gamma n$ reaction and disappears in the shapes of coherent and incoherent $\gamma D$ reactions, modifying the absolute values of the two latter ones. Since there is no pure neutron

target, one must analyze the difference in unpolarized $\gamma p$ and $\gamma D$ reactions. This effect is expected on the level of 5–10%, and it is hardly to be seen in available data with their present resolution. Therefore, to be sure of the existence of such an irregular behavior, the experimental resolution of the data around $E_\gamma \sim 2$ GeV must be greatly improved by providing additional information on the channels with spin- and double-spin-flip transitions which are sensitive to properties of the photoproduction amplitude in $\gamma p$ and $\gamma D$ reactions. This problem may be studied experimentally at the electron and photon facilities at LEPS and JLab, the crystal barrel detector at ELSA (electron stretcher and accelerator) at the Physics Institute, Bonn University, and the Graal $\gamma$-ray beam of the European Synchrotron Radiation Facility in Grenoble.

## ACKNOWLEDGMENTS

We thank W.C. Chang, S. Daté, H. Ejiri, M. Fujiwara, T. Mibe, T. Nakano, and Y. Ohashi for many fruitful discussions and comments. A.I.T. also thanks colleagues at FZD for their hospitality. This work was supported by BMBF Grant 06DR136 and GSI-FE.

[1] T. Nakano and H. Toki, in *Proceedings of the International Workshop on Exiting Physics and New Accelerator Facilities*, SPring-8, Hyogo, 1997 (World Scientific, Singapore, 1998), p. 48.
[2] M. A. Pichowsky and T.-S. H. Lee, Phys. Rev. D **56**, 1644 (1997).
[3] A. I. Titov, Y. Oh, S. N. Yang, and T. Morii, Phys. Rev. C **58**, 2429 (1998).
[4] Q. Zhao, Z. Li, and C. Bennhold, Phys. Lett. **B436**, 42 (1998); Phys. Rev. C **58**, 2393 (1998).
[5] R. A. Williams, Phys. Rev. C **57**, 223 (1998).
[6] J.-M. Laget, Phys. Lett. **B489**, 313 (2000).
[7] A. I Titov and T.-S. H. Lee, Phys. Rev. C **67**, 065205 (2003).
[8] A. Donnachie and P. V. Landshoff, Phys. Lett. **B185**, 403 (1987); Nucl. Phys. **B244**, 322 (1984); **B267**, 690 (1986).
[9] M. G. Ryskin, Z. Phys. C **57**, 89 (1993).
[10] J. R. Cudell and I. Royen, Phys. Lett. **B397**, 317 (1997).
[11] T. Mibe *et al*. (LEPS Collaboration), Phys. Rev. Lett. C **95**, 182001 (2005).
[12] L. L. Frankfurt, J. Mutzbauer, W. Koepf, G. Piller, M. Sargsian, and M. I. Strikman, Nucl. Phys. **A622**, 511 (1997); L. Frankfurt, G. Piller, M. Sargsian, and M. Strikman, Eur. Phys. J. A **2**, 301 (1998).
[13] T. C. Rogers, M. M. Sargsian, and M. I. Strikman, Phys. Rev. C **73**, 045202 (2006).
[14] A. I. Titov, M. Fujiwara, and T. S.-H. Lee, Phys. Rev. C **66**, 022202(R) (2002).
[15] W. C. Chang *et al*. (LEPS Collaboration), arXiv:nucl-ex/0703034.
[16] T. Mibe *et al*. (CLAS Collaboration), arXiv:nucl-ex/0703013.
[17] P. V. Landshoff and O. Nachtmann, Z. Phys. C **35**, 405 (1987).
[18] S. L. Zhu, Phys. Rev. C **61**, 065205 (2000).
[19] J. Piekarewicz, Phys. Rev. C **48**, 1555 (1993).
[20] L. Tiator, C. Bennhold, and S. S. Kamalov, Nucl. Phys. **A580**, 455 (1994); M. Kirchbach and L. Tiator, *ibid*. **A604**, 385 (1996).
[21] A. I. Titov, T.-S. H. Lee, H. Toki, and O. Streltsova, Phys. Rev. C **60**, 035205 (1999).
[22] J. Barth *et al*., Eur. Phys. J. A **17**, 269 (2003).
[23] H. J. Besch *et al*., Nucl. Phys. **B70**, 257 (1974).
[24] E. Anciant *et al*. (CLAS Collaboration), Phys. Rev. Lett. **85**, 4682 (2000).
[25] Durham data base. http://www.slac.stanford.edu/spires/hepdata/.
[26] M. Lacombe, B. Loiseau, R. Vinh Mau, J. Cote, P. Pires, and R. de Tourreil, Phys. Lett. **B101**, 139 (1981).
[27] M. Lacombe, B. Loiseau, J. M. Richard, R. Vinh Mau, J. Conte, P. Pires, and R. de Tourreil, Phys. Rev. C **21**, 861 (1980).
[28] W. C. Chang provided us with the $[\gamma D, \phi]$ missing mass distribution at $\Delta_t = 0$–$0.1$ GeV$^2$, measured by the LEPS Collaboration (private communication).
[29] K. Schilling, P. Seyboth, and G. E. Wolf, Nucl. Phys. **B15**, 397 (1970); erratum-*ibid*. **B18**, 322 (1980).
[30] T. Mibe provided us with the experimental data of the angular distribution $W^L(\Phi - \Phi)$ for the $\gamma p \to \phi p$ reaction measured by the LEPS Collaboration (private communication).